THE JOURNAL OF PHYSICAL CHEMISTRY B

Article

pubs.acs.org/JPCB

Ion Jelly Conductive Properties Using Dicyanamide-Based Ionic Liquids

Tânia Carvalho,[†] Vera Augusto,[†] Ângelo Rocha,[§] Nuno M. T. Lourenço,[§] Natália T. Correia,[$] Susana Barreiros,[†] Pedro Vidinha,[†,#] Eurico J. Cabrita,[†] and Madalena Dionísio*[,†]

[†]REQUIMTE/CQFB, Departamento de Química, Faculdade de Ciências e Tecnologia da Universidade Nova de Lisboa, 2829-516 Caparica, Portugal

[§]IBB-Institute for Biotechnology and Bioengineering, Centre for Biological and Chemical Engineering, Instituto Superior Técnico, Av. Rovisco Pais, 1049-001 Lisboa, Portugal

[$]Unité Matériaux et Transformation (UMET), UMR CNRS 8207, UFR de Physique, BAT P5, Université Lille 1, 59655 Villeneuve d'Ascq, France

[#]Instituto de Química, Universidade de São Paulo, Av. Prof. Lineu Prestes, 748, CEP 05508-000, São Paulo, SP, Brazil

ABSTRACT: The thermal behavior and transport properties of several ion jellys (IJs), a composite that results from the combination of gelatin with an ionic liquid (IL), were investigated by dielectric relaxation spectroscopy (DRS), differential scanning calorimetry (DSC), and pulsed field gradient nuclear magnetic resonance spectroscopy (PFG NMR). Four different ILs containing the dicyanamide anion were used: 1-butyl-3-methylimidazolium dicyanamide (BMIMDCA), 1-ethyl-3-methylimidazolium dicyanamide (EMIMDCA), 1-butyl-1-methylpyrrolidinium dicyanamide (BMPyrDCA), and 1-butylpyridinium dicyanamide (BPyDCA); the bulk ILs were also investigated for comparison. A glass transition was detected by DSC for all materials, ILs and IJs, allowing them to be classified as glass formers. Additionally, an increase in the glass transition temperature upon dehydration was observed with a greater extent for IJs, attributed to a greater hindrance imposed by the gelatin matrix after water removal, rendering the IL less mobile. While crystallization is observed for some ILs with negligible water content, it was never detected for any IJ upon thermal cycling, which persist always as fully amorphous materials. From DRS measurements, conductivity and diffusion coefficients for both cations (D_+) and anions (D_-) were extracted. D_+ values obtained by DRS reveal excellent agreement with those obtained from PFG NMR direct measurements, obeying the same VFTH equation over a large temperature range ($\Delta T \approx 150$ K) within which D_+ varies around 10 decades. At temperatures close to room temperature, the IJs exhibit D values comparable to the most hydrated (9%) ILs. The IJ derived from EMIMDCA possesses the highest conductivity and diffusion coefficient, respectively, $\sim 10^{-2}$ S·cm^{-1} and $\sim 10^{-10}$ m^2·s^{-1}. For BMPyrDCA the relaxational behavior was analyzed through the complex permittivity and modulus formalism allowing the assignment of the detected secondary relaxation to a Johari−Goldstein process. Besides the relevant information on the more fundamental nature providing physicochemical details on ILs behavior, new doorways are opened for practical applications by using IJ as a strategy to produce novel and stable electrolytes for different electrochemical devices.

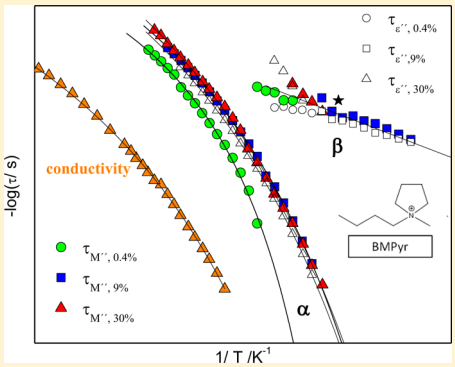

INTRODUCTION

The research on ionic liquids (ILs) has grown exponentially in the last two decades due to their unique physical-chemical properties that enable their application in a broad range of scientific fields. ILs are comprised entirely by ions and most of them exhibit a negligible vapor pressure, ionic conductivity, and a high thermal, chemical, and electrochemical stability.[1−3] Nevertheless the tailor-made design of ILs is probably the most fascinating and creative domain on ILs research. In fact the creative design of ILs has driven their application to completely different areas such as in physics or biology. For the design, however, it is imperative to evaluate the fundamental physical-chemical properties before trying to evolve a given IL structure for a particular application. For instance, the type of molecular interaction between cation and anion is determinant for physical-chemical properties such as melting temperature, glass transition temperature, or conductivity.[4]

The development of ILs based materials is a promising field of research for the design of new advanced functional tailor-made materials. In particular, ILs gelation induced by polymers originates quasi-solid materials commonly called ion gels which are very interesting, offering good mechanical strength and conductivity.[5] Indeed, ion gels hold both the processability and mechanical properties of polymers, but with added phys-

Received: March 22, 2014
Revised: June 5, 2014
Published: July 24, 2014

   dx.doi.org/10.1021/jp502870q | J. Phys. Chem. B 2014, 118, 9445−9459

icochemical properties and although primarily developed as replacements for current solid-state polyelectrolytes.[6] Several other applications are currently emerging as in sensors[7] and drug delivery applications.[8]

In general, the methods to prepare IL-based polymer gels can be classified into three major types: gelation of ILs within polymers/biopolymers, in situ polymerization of vinyl monomers in ILs, and polymerization of ILs containing polymerizable groups (e.g. vinyl groups).[9−11]

The introduction of polymerizable groups into the IL structure has been presented as a very interesting way to obtain good ionic conductivity without liquid components. These polymerized ionic liquids (PILs) have been developed for battery electrolyte and for other solid electrolyte applications.[12−15] Nevertheless on polymeric lithium batteries besides a good conductivity it is necessary that specific molecules like the lithium ion can be easily transported through the electrolyte. Combining these two factors on PILs is not a simple task since the variables, conductivity and ion transport, are related with several issues (e.g., type of cation and anion and viscosity).

Following the trend of IL gelation we reported ion jelly (IJ), a light flexible electrolyte that results from the combination of gelatin with an IL.[16] This allows the production of gels that are extremely versatile conductive materials that can be molded into different shapes, using several techniques, and can be adapted to multiple surfaces. Moreover, on cooling, IJ can undergo a liquid-gel transition near room temperature (near 35 °C), which makes a promising solution to develop electrolyte "inks" for printed electrochemical devices. We have also shown that IJ could have multiple applications and could be produced in different forms.[17−19]

However, the evaluation of basic thermophysical properties is vital to the design of IJs and to conceive a given application on electrochemical devices. For that purpose, it is essential to understand the physicochemical behavior of ILs in an IJ matrix. To accomplish this goal, we have recently reported a study that led to the basic understanding of a IJ conductive mechanism, by means of dielectric relaxation spectroscopy (DRS)[21] that, for a sample under the influence of an oscillating electrical field, probes reorientational movements of dipoles, interfacial polarization, and propagation of mobile charge carriers. The charge carrier's migration is due to translational diffusion through hopping movements of electrons, holes, and ions giving rise to conductivity and allowing information to be obtained on charge transport properties. While dipolar reorientations are usually probed through the complex dielectric function, $\varepsilon^*(\omega)$, conductivity is monitored by the complex electric conductivity $\sigma^*(\omega) = \sigma'(\omega) + i\sigma''(\omega)$, where σ' and σ'' are the corresponding real and imaginary parts. The two properties are related by $\sigma^*(\omega) = i\omega\varepsilon_0\varepsilon^*(\omega)$.[20]

Through this approach, where the estimated diffusion coefficients were compared with those measured by pulsed-filed gradient NMR (PFG-NMR),[21] it was possible to illustrate the impact of gelatin and water on IL physicochemical properties, which were ultimately implicated on IJ conductivity. In this particular case it was found that IJ with a higher IL/gelatin ratio exhibits identical conductive properties to BMIMDCA meaning that the ionic conductivity is not significantly affected by the presence of gelatin. Nevertheless, an increase in the amount of gelatin led to a decrease on the IJ conductivity showing that there is a critical ratio of IL/gelatin that leads to those properties.

Additionally, the thermal behavior of both IL precursors and corresponding IJs is investigated to analyze the respective phase transformations: glass transition, crystallization, and melting. Crystallization and vitrification are complex phenomena that could be either driven or avoided by different thermal treatments. We found that ILs are suitable models to understand these physical changes.

Nevertheless there were still some questions that remained to be addressed: Could the changes on cation produce a significative impact on the interaction between IL and gelatin? Or could it be possible to produce an IJ with a higher conductivity than the bulk IL? To address these questions we have used four different ILs containing the dicyanamide anion: 1-butyl-3-methylimidazolium dicyanamide (BMIMDCA), 1-ethyl-3-methylimidazolium dicyanamide (EMIMDCA), 1-butyl-1-methylpyrrolidinium dicyanamide (BMPyrDCA), and 1-butylpyridinium dicyanamide (BPyDCA). All the dicyanamide (DCA) compounds were liquid at room temperature and characterized by water miscibility. Moreover, the dicyanamide ion is an anionic bridge ligand that has Lewis base attributes, which makes it particularly attractive to synthesize ILs with very specific properties. Compared to common anions such as PF_6 or BF_4, DCA has a permanent dipole and thus facilitates the research on IL dynamics through dielectric spectroscopy.[22,23]

EXPERIMENTAL SECTION

Materials. The room temperature ILs—1-butyl-3-methylimidazolium dicyanamide (BMIMDCA), 1-butyl-1-methylpyrrolidinium dicyanamide (BMPyrDCA), and 1-ethyl-3-methylimidazolium dicyanamide (EMIMDCA)—were provided by Iolitec, with purity >98%, with the properties and reference numbers as given in Table 1.

Table 1. Physical Properties of Ionic Liquids: Molar Weight (MW) and Density (Water Percentage Is Also Provided)[a]

	BMIMDCA	BMPyrDCA	EMIMDCA
Iolitec ref	IL-0010-HP	IL-0041-HP	IL-0003-HP
MW	205.26	208.30	177.21
density$_{298K}$/g·cm^{-3}	1.058[24]	1.013[25]	1.060[1]
water % (w/w)	0.4	0.4	0.4

[a]1-Butylpyridinium dicyanamide (BPyDCA) was synthesized by A. Rocha having MW of 203.27.

The cation chemical structures are shown is Scheme 1 together with van der Waals radius and volume estimated by using Spartan.[26]

Ion Jelly Preparation. To prepare the respective ion jelly (IJ), 300 μL of each neat IL was heated to 313 K under magnetic stirring, followed by the addition of 120 mg of gelatin,

Scheme 1. Cation Chemical Structures with the Respective van der Waals Radius (r) and Volume (V)

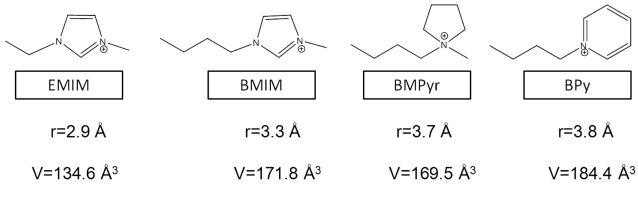

Gelatin was purchased from Panreac ref 403 902. All materials were used as received.

dx.doi.org/10.1021/jp502870q | J. Phys. Chem. B 2014, 118, 9445−9459

giving an approximate ratio of 3:1 IL/gelatin (w/w). To obtain a homogeneous solution, 75 μL of water was added dropwise. The mixtures were stirred at 313 K until the gelatin was completely solubilized (approximately 15 min). The solutions were then spread over a glass surface to form thin films. Jellification occurred at room temperature. The designation used for the different IJ materials is Ionic_liquid$_{IJ}$.

Therefore, 12 systems were tested in the present work: BPyDCA$_{0.4\%}$, BPyDCA$_{9\%}$, BPyDCA$_{IJ}$, BMIMDCA$_{0.4\%}$, BMIMDCA$_{9\%}$, BMIMDCA$_{IJ}$, BMPyrDCA$_{0.4\%}$, BMPyrDCA$_{9\%}$, BMPyrDCA$_{IJ}$, EMIMDCA$_{0.4\%}$, EMIMDCA$_{9\%}$, and EMIMDCA$_{IJ}$.

Karl Fischer titration (813 KF coulometer from Metrohm) was used to determine the water content in each final material prior to use (see Table 1 for the water content in the neat ILs); the water content in the IJ materials is 9% independently of the IL used. Therefore, to compare conductive properties, ILs with the 9% water amount were prepared, which will be designated hereafter as IL$_{9\%}$; additionally to elucidate the secondary relaxation process detected in the as prepared IL, BMPyrDCA was prepared with 30% (w/w) water content: BMPyrDCA$_{30\%}$.

Techniques. *Differential Scanning Calorimetry.* The calorimetric experiments were carried out with a DSC Q2000 from TA Instruments Inc. (Tzero DSC technology) operating in the Heat Flow T4P option (details can be found in ref 27); at least two scans at a cooling and heating rate of 20 deg·min^{-1} were performed covering the temperature range from 123 to 423 K for each system; each sample was kept 5 min at 423 K at the end of the first scan to ensure water removal. The relatively high heating rate was used to increase the sensitivity of the calorimetric signal to enhance the heat capacity jump, which is quite broad for the IJ materials.

Measurements were realized under dry high purity helium at a flow rate of 50 mL·min^{-1}; a liquid nitrogen cooling system (LNCS) was used to reach temperatures as low as 123 K. DSC Tzero calibration was carried out in the temperature range from 108 to 573 K. It requires two experiments: the first run with the empty cell (baseline) and the second run with equal weight sapphire disks on the sample and reference platforms (without pans). This procedure allows for cell resistance and capacitance calibration which compensates for subtle differences in thermal resistance and capacitance between the reference and sample platforms in the DSC sensor. Enthalpy (cell constant) and temperature calibration were based on the melting peak of indium standard (T_m = 429.75 K) supplied by TA Instruments (Lot No. E10W029). Less than 7 mg of each sample was encapsulated in Tzero (aluminum) hermetic pans with a Tzero hermetic lid with a pinhole to allow water to escape by evaporation.

Dielectric Relaxation Spectroscopy. For the dielectric spectroscopy measurements, IJ films were cut into disks of about 10 mm in diameter. The films thickness varies between 0.5 and 0.7 mm; no thinner films were possible to obtain being the thickness limited by the formation of a self-supported gelatin film. For the ILs measurements (both 0.4% and 9% water), two silica spacers of 0.05 mm thickness were used. The samples were placed between two stainless steel electrodes (the smaller electrode had a 10 mm diameter) in a parallel plate capacitor, BDS 1200. The sample cell was mounted on a cryostat, BDS 1100, and exposed to a heated gas stream being evaporated from liquid nitrogen in a Dewar. The temperature control was assured by the Quatro Cryosystem and performed within ±0.5 K (all modules supplied by Novocontrol). Measurements were carried out with an Alpha-N analyzer also from Novocontrol GmbH, covering a frequency range from 10^{-1} Hz to 1 MHz.

All samples were submitted to the same thermal treatment. After a first cooling ramp from room temperature to 163 K, isothermal spectra were collected upon increasing different temperature steps: in the range 163 K $\leq T \leq$ 213 K each spectrum was recorded every 2 K; from 213 to 313 K the spectra were recorded every 5 K.

DRS Data Treatment. As mentioned in the Introduction, the material can respond to the applied electrical field by means of dipolar reorientations, probed through the complex dielectric function, $\varepsilon^*(\omega)$, which can be simulated by the model function introduced by Havriliak−Negami:[28,29]

$$\varepsilon^*(f) = \varepsilon_\infty + \frac{\Delta\varepsilon}{[1 + (i\omega\tau_{HN})^{\alpha_{HN}}]^{\beta_{HN}}} \quad (1)$$

where, $\Delta\varepsilon = \varepsilon_s - \varepsilon_\infty$ is the dielectric strength, i.e., the difference between the real permittivity values at respectively the low and high frequency limits, τ_{HN} is the relaxation time, and α_{HN} and β_{HN} are the shape parameters ($0 < \alpha_{HN} < 1$; $0 < \alpha_{HN}\beta_{HN} < 1$). Since data are strongly influenced by the low frequency conductivity contribution, an additional term $i\sigma/\omega^c\varepsilon_0$ was added to the dielectric loss, where ε_0 is the vacuum permittivity; σ and c are fitting parameters: σ is related to the dc conductivity of the sample, and the parameter c ($0 < c \leq 1$) reflects conductivity of ions for $c = 1$ and for $c < 1$ interfacial polarizations, including electrode polarization.

The nonlinear temperature dependence of the relaxation times usually associated with the dynamic glass transition process obeys the Vogel/Fulcher/Tammann/Hesse (VFTH) equation,[30−32] which also describes quite well the temperature dependence of conductivity, reading respectively as

$$\tau(T) = \tau_\infty \exp\left(\frac{B}{T - T_0}\right) \quad (2a)$$

$$\sigma_0(T) = \sigma_\infty \exp\left(-\frac{B}{T - T_0}\right) \quad (2b)$$

where τ_∞ and σ_∞ are the values of the relaxation time and conductivity in the high temperature limit, B is an empirical parameter characteristic of the material accounting for the deviation of linearity (roughly the lower B the more curved is the $1/T$ plot), and T_0 is the Vogel temperature, interpreted, for the equation expressed in relaxation time (eq 2a), as the glass transition temperature of an ideal glass, i.e., a glass obtained with an infinitely slow cooling rate.[33]

Nuclear Magnetic Resonance. NMR spectra were recorded on a Bruker Avance III 400 spectrometer, operating at 400.15 MHz, equipped with pulse gradient units, capable of producing magnetic field pulsed gradients in the z direction of 0.54 T·m^{-1}. Diffusion measurements were performed by using the stimulated echo sequence, using bipolar sine gradient pulses and eddy current delay before the detection.[34] The signal attenuation is given by

$$S = S_0 \exp\left(-\gamma^2 g^2 D\delta^2\left(\Delta - \frac{2\delta}{3} - \frac{\tau_g}{2}\right)\right) \quad (3)$$

where D denotes the self-diffusion coefficient, γ the gyromagnetic ratio, δ the gradient pulse width, Δ the diffusion time, τ_g the gradient recovery delay, and g the gradient strength

dx.doi.org/10.1021/jp502870q | J. Phys. Chem. B 2014, 118, 9445−9459

corrected according to the shape of the gradient pulse. Before all NMR experiments, the temperature was equilibrated and maintained constant within ±0.1 K, as measured using the spectrometer thermocouple system. Experiments were performed at 298.15, 288.15, 278.15, 273.15, 268.15, 258.15, 253.15, and 248.15 K. The spectra were recorded in 5 mm NMR tubes with an air flow of 535 L h^{-1}.

Typically, in each experiment, a number of 32 spectra of 32 K data points were collected, with values for the duration of the magnetic field pulse gradients (δ) of 2.5 to 3.5 ms, diffusion times (Δ) of 400 to 2000 ms, and an eddy current delay set to 5 ms; the gradient recovery time (τ_g) was 200 μs. The sine-shaped pulsed gradient (g) was incremented from 5% to 95% of the maximum gradient strength in a linear ramp. The spectra were first processed in the F2 dimension by standard Fourier transform and baseline correction with the Bruker Topspin software package (version 2.1). The diffusion coefficients are calculated by exponential fitting of the data belonging to individual columns of the 2D matrix. The diffusion coefficients (D) were obtained by measuring the signal intensity at more than one place in the spectra. At least two different measurements were done for the determination of each diffusion coefficient.

RESULTS AND DISCUSSION

Thermal Characterization. Differential scanning calorimetry (DSC) was used to probe ILs and IJs thermal transitions over several scans (see the Experimental Section). For all the materials, a broad and endothermic peak which onset is located around 300 K is detected in the first scan corresponding to water evaporation being absent in the subsequent runs after water removal. Figure 1 illustrates this effect for $BMPyrDCA_{9\%}$ (green line).

At lower temperatures (close to 170 K for BMPyrDCA in Figure 1), a discontinuity in the heat flux is observed in both scans due to the glass transition. However, in the second scan this heat flux step is shifted toward higher temperatures (green vs pink solid line). This means that the glass transition temperature decreases upon hydration due to a plasticizing effect of water, as already observed by some of us for BMIMDCA[21] and by Troshenkova et al.[35] for aqueous mixtures of 1-ethyl-3-methylimidazolium acetate up to 40% (w/w). This is observed for all the ILs and IJ studied in the present work; for BMPyrDCA and EMIMDCA the shift is close to 20 K. However, this is not a universal behavior as reported in ref 36 for ILs incorporating the imidazolium cation where the shift upon hydration is toward higher temperatures, revealing an antiplasticizing effect, but in less extent (ΔT = 2−7 K).

The detection in each system of a glass transition from which a T_g can be determined allows us to classify all the tested materials as glass formers.

Moreover, for $BMPyrDCA_{9\%}$ (pink solid line in Figure 1) it is possible to see three distinct transformations in the thermogram obtained in the second scan for the dehydrated IL: the glass transition, an exothermic peak indicating crystallization, and an endothermic peak corresponding to melting; the same behavior occurs for EMIMDCA after water removal irrespective to the initial water content (Figure 2).

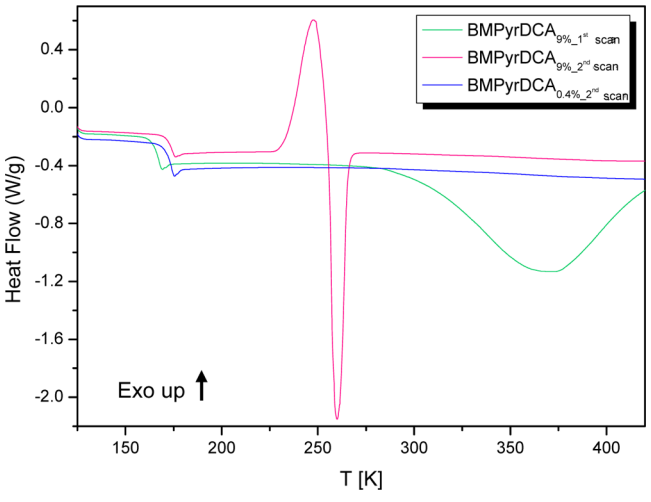

Figure 1. Thermograms collected upon heating at 20 K·min^{-1} for BMPyrDCA with different water contents and over different scans. The broad endotherm centered at ~370 K is due to water evaporation and the discontinuity at lower temperatures is due to the glass transition; the sharp exo- and endotherms in the thermogram of $BMPyrDCA_{9\%\_2^{nd}scan}$ (pink line) are due to crystallization and melting, respectively; no thermal events other than glass transition were observed in the initial cooling run.

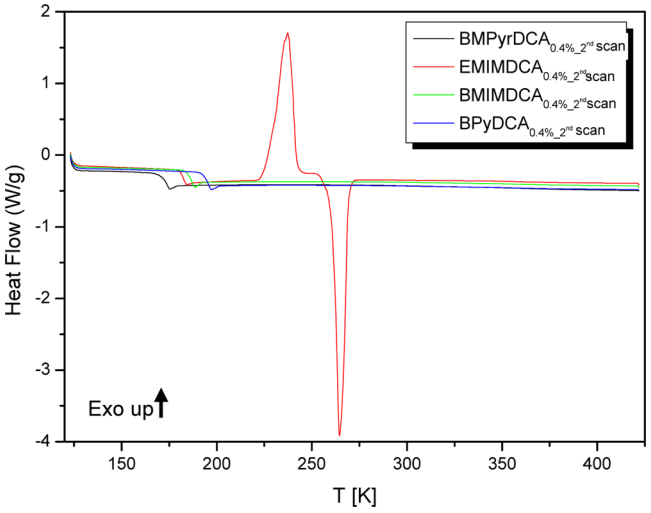

Figure 2. Thermograms collected upon heating at 20 K·min^{-1} for all tested ILs after dehydration (2nd scan). At the lowest temperatures the different location of the heat flow step due to glass transition is evident; sharp exo- and endotherms in the thermogram of $EMIMDCA_{0.4\%\_2^{nd}scan}$ (red line) are due to crystallization and melting, respectively.

Oppositely, for $BMPyrDCA_{0.4\%}$ after heating to 363 K (2nd scan) no crystallization is observed (blue line in Figure 1), although the heat flux jump due to glass transition occurs at the same temperature as for dehydrated (2^{nd} scan) $BMPyrDCA_{9\%}$, as expected. The nonreproducibility of phase transformations for the same IL was already found for BMIMDCA: samples taken from a different batch and reported in refs 21 and 24 exhibit crystallization, opposite what is observed in the present work. Even so, the water removal seems to be a condition for crystallization to occur. Identical behavior was observed for ultrapure 1-ethyl-3-methylimidazolium chloride after the draining of the liquid residue[37] indicating a strong spatial ordering of the ions forming a crystal lattice. The temperatures of the minimum/maximum of melting and crystallization peaks, for the cases where they are observed, are included in Table 2.

dx.doi.org/10.1021/jp502870q | J. Phys. Chem. B 2014, 118, 9445−9459

Table 2. Glass Transition Temperatures Taken at the Onset (on), Midpoint (mid), and Endset (end) of the Heat Flow Jump for $BPyDCA_{9\%water}$, $BMIMDCA_{9\%water}$, $BMPyrDCA_{9\%water}$, $EMIMDCA_{9\%water}$, and Respective IJ, Obtained during a First Heating Run at 20 K·min^{-1} with Melting and Crystallization Temperatures Obtained from a Second Heating Run

system	heating run	$T_{g,on}$/K	$T_{g,mid}$/K	$T_{g,end}$/K	T_c/K	T_m/K
$BPyDCA_{9\%water}$	1st	175.4	177.8	179.0		
	2nd	194.9	197.2	197.9		
$BPyDCA_{IJ}$	1st	185.4	189.6	213.4		
	2nd	213.9	227.1	249.8		
$BMIMDCA_{9\%water}$	1st	169.0	171.5	172.3		
	2nd	185.4	187.4	188.1		
$BMIMDCA_{IJ}$	1st	174.2	176.5	182.3		
	2nd	196.8	200.4	206.4		
$BMPyrDCA_{9\%water}$	1st	164.4	167.5	168.2		
	2nd	171.7	174.6	171.5	247.9	260.0
$BMPyrDCA_{IJ}$	1st	170.5	173.9	180.1		
	2nd	188.0	198.7	220.5		
$EMIMDCA_{9\%water}$	1st	161.9	164.2	164.5		
	2nd	180.1	182.6	182.8	225.7	263.2
$EMIMDCA_{IJ}$	1st	166.2	168.4	174.8		
	2nd	191.1	195.1	203.0		

Figure 2 shows the thermograms obtained after dehydration (2nd scans) for the studied set of ILs. To simplify the comparison between all systems, the BMPyrDCA sample included in the figure is the one having initially 0.4% water undergoing no crystallization; for dehydrated (2nd scan) EMIMDCA (red line) crystallization is observed, as mentioned above. The glass transition occurs at different temperatures for each IL, being lower for BMPyrDCA (black line) and higher for BPyDCA (blue line). A more detailed discussion will be carried out later in the paper.

The temperature values extracted from the onset, the midpoint, and the endset of the glass transition for ILs after water removal are presented in Table 2 (values taken from the first scan are also included).

In regard to IJ materials, which initial water content is 9%, the glass transition temperature is also influenced by the amount of incorporated water. Figure 3 illustrates this for $BMIMDCA_{IJ}$ (gray and green lines), for which the heat flux jump due to the glass transition detected in the first scan significantly deviates to higher temperatures in the second scan ($\Delta T \approx 24$ K); above 300 K the first thermogram unravels the water evaporation by the emergence of a broad endotherm. The shift in the glass transition upon water removal is even higher than the one observed for the respective IL; this occurs for all IJs. Moreover, the heat flux jump is broader and less pronounced for the IJs compared with the respective ILs. The comparison between the glass transition observed for dehydrated $BPyDCA_{IJ}$ and respective IL is done in the inset of Figure 3, illustrating these features.

The T_g values extracted from the onset, the midpoint, and the endset of the IJs glass transition are included in Table 2. Since the width of the transition for the IJs covers a relatively wide temperature range, the T_g value used to compare the glass transition temperature between the different materials is the one determined from the onset of the calorimetric signal as adopted in ref 21. Taken as $T_{g,on}$, it is clear that occurs at different temperatures for each IJ, obeying the same order as observed for the dehydrated ILs.

Additionally, the T_g values for the IJs are always higher than the corresponding T_g for the respective ILs, which will be confirmed later on by DRS for the hydrated materials, both IL and IJ containing 9% water. This may indicate that not all the water in the IJ composites is interacting directly with the IL, being partionated between the IL and gelatin assuring its structure. Additionally, some hindrance can be caused by the rigidity of the matrix at these low temperatures that manifest in a greater extent for the dehydrated materials. In fact, the water removal may increase the stiffness of the gelatin matrix hindering even more the mobility of the entrapped IL increasing its glass transition temperature.

Furthermore, none of the IJ material undergoes crystallization, which means that these materials are fully amorphous.

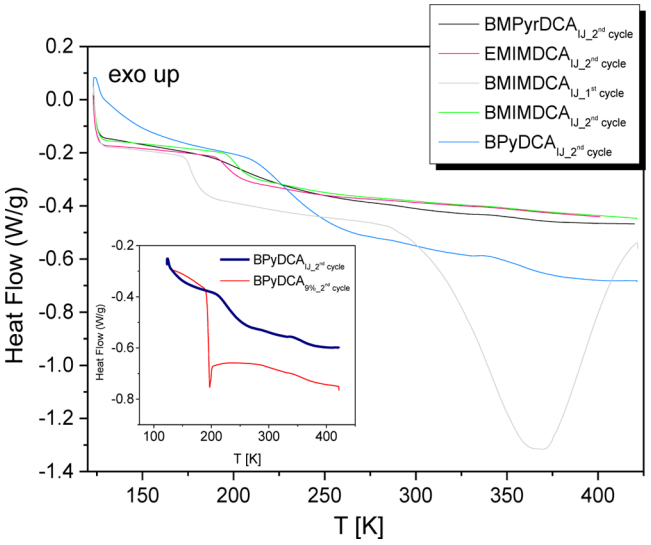

Figure 3. Thermograms for the different IJs (see legend) taken upon heating at 20 K·min^{-1}. The gray and green lines show the 1st and 2nd scans, respectively, for BMIMDCA evidencing the significant shift to high temperatures of the glass transition upon water removal; the broad and intense endotherm centered around 373 K is due to water evaporation (1st scan). In the inset, the thermograms (2nd scan) for BPyDCA, IL, and IJ are displayed illustrating the broadening of the heat flux step at the glass transition being also less pronounced and shifted to higher temperatures for the IJ as compared with bulk IL; the thermogram for the IJ (thicker upper trace) was vertically displaced to allow a better comparison.

dx.doi.org/10.1021/jp502870q | J. Phys. Chem. B 2014, 118, 9445−9459

DIELECTRIC CHARACTERIZATION

Conductivity and Transport Properties. The complex conductivity of the 12 materials was measured from 10^{-1} to 10^{6} Hz and covering a range of temperatures from 163 to 298 K; its real component is shown in Figure 4a,b for $BPyDCA_{0.4\%}$ and

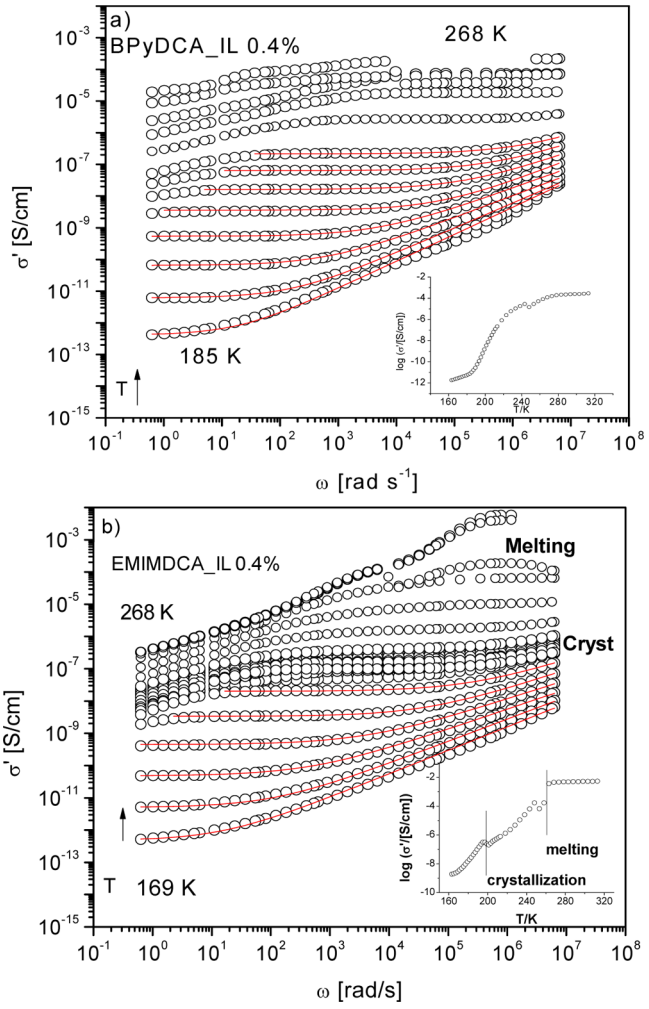

Figure 4. Real part of conductivity for (a) $BPyDCA_{IL0.4\%}$ and (b) $EMIMDCA_{IL0.4\%}$. The solid lines are the obtained fits by the Jonscher law (eq 4) for isotherms in steps of 4 deg between 185 and 231 K for $BPyDCA_{IL0.4\%}$ and between 169 and 189 K for $EMIMDCA_{IL0.4\%}$. The isotherms presented here for the highest temperatures, in both systems, were taken from 213 to 243 K in steps of 10 deg, and between 258 and 268 K in steps of 5 deg; in panel b, the isotherms between 201 and 211 K in steps of 2 deg were included to illustrate the crystallization effect. The insets are the isochronal plots of the conductivity at (a) 10^2 and (b) 4×10^5 Hz.

for the crystallizable $EMIMDCA_{0.4\%}$. It is interesting to note how crystallization affects the conductivity spectrum of EMIMDCA as seen by a sudden drop just above 200 K in the isochronal conductivity plot at $\nu = 4 \times 10^5$ Hz presented in the inset of Figure 4b; the increase at 263 K is due to melting. The latter temperature transition is in very good agreement with the minimum of the melting peak detected calorimetrically; the same is not completely true for the crystallization which is not fully unexpected since kinetic factors also contribute for this transition with the cooling/heating rate, and experimental setup as well, being different from the DSC conditions; nevertheless for the sample containing initially 9% water the onset of crystallization after water removal occurs at 216 K very near what is observed for this sample. It is worth mentioning that in the first run no crystallization was observed for any IL by DSC. The detection of crystallization for $EMIMDCA_{0.4\%}$ by dielectric spectroscopy may be due to an efficient water removal by the nitrogen flux that controls the temperature in the sample holder. This may occur when the sample is kept close to room temperature before cooling.

Both real and imaginary parts of the complex permittivity (not shown) are also sensitive to crystallization. Therefore, DRS is a suitable tool to monitor crystallization through the isochronal conductivity plot in these relatively high conducting disordered systems.

BPyDCA fails to crystallize as was concluded by DSC; only electrical anomalies manifest at high frequencies as commonly observed in ILs, being the origin of the small discontinuity in the isochronal conductivity plot at $\nu = 1 \times 10^2$ Hz presented in the inset of Figure 4a. As noted in a previous publication,[21] the IJs dielectric measurements are not affected by these interferences nor by crystallization being much more stable relative to the bulk ILs.

An important feature in the spectral region under study is the detection of a plateau in $\sigma'(\nu)$, which gives σ_0, the dc conductivity; ν is the frequency of the applied oscillating electrical field. At the lowest temperatures, or high frequencies, the conductivity becomes frequency dependent and the $\sigma'(\nu)$ plot presents a pronounced increase. Additionally, a decrease is observed in real conductivity at the lowest frequencies and higher temperatures due to electrode polarization as found in similar materials;[38] this means that ionic conduction becomes blocked, i.e., ions accumulate in the sample/electrode interface without discharging.

The characteristic crossover frequency, $\omega_{cross} = 2\pi\nu_{cross}$, is the frequency at which the plateau bends off to the frequency dependent region, separating into two diffusive regimes that are related to the time dependence of the mean-square displacement, $\langle \Delta r^2(t) \rangle$, which is of the order of the distance that a particle can jump when diffusing in a time $t^* = 1/\nu_{cross}$.[21,39] If the measurements are taken over large time scales/low frequencies, $\omega < \omega_{cross}$, the mean square displacement of ions during charge transport varies linearly with time ($\langle \Delta r^2(t) \rangle \propto t$)[39] and the conductivity is frequency independent, all σ' values falling in a plateau. Under these conditions, the conductivity properties are governed by diffusive movements of ions. On the other hand, for short time scales/high frequencies for which $\omega > \omega_{cross}$, the movement of ions is subdiffusive, which means that the mean-square displacement increases sublinearly with time,[40] $\langle \Delta r^2(t) \rangle \propto t^{0.35}$,[39] and the conductivity increases with frequency.

At the lowest temperatures, the regime is permanently subdiffusive and no crossover is observed.

It is interesting to observe that there is some correlation between the temperature at which a plateau starts to emerge in the frequency-dependent real conductivity plot and the onset of the calorimetric glass transition temperature, ($T_{g,DSC}$); this was reported previously by some of us for related systems.[21] Figure 5 presents a comparison between those two temperature values showing a relatively good agreement, which provides a mean to roughly estimate the glass transition temperature from conductivity measurements. The highest deviation between the temperature values estimated by DRS and those

dx.doi.org/10.1021/jp502870q | J. Phys. Chem. B 2014, 118, 9445−9459

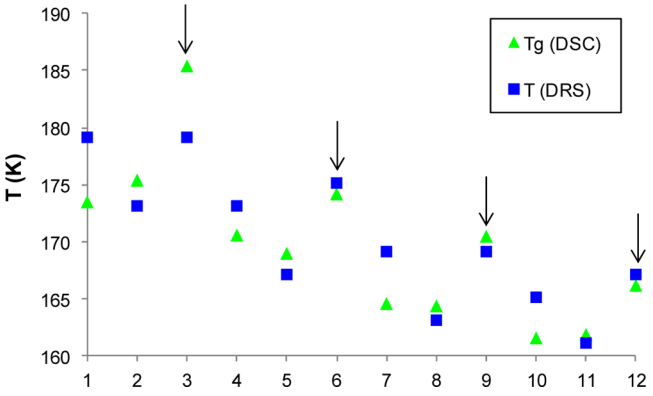

Figure 5. Correlation between the T_g extracted from DSC (in green) and the temperature at which a plateau starts to emerge in the log(σ) vs ν plot, estimated from spectra collected by DRS (in blue): 1-$BPyDCA_{0.4\%}$, 2-$BPyDCA_{9\%}$, 3-$BPyDCA_{IJ}$; 4-$BMIMDCA_{0.4\%}$, 5-$BMIMDCA_{9\%}$, 6-$BMIMDCA_{IJ}$; 7-$BMPyrDCA_{0.4\%}$, 8-$BMPyrDCA_{9\%}$, 9-$BMPyrDCA_{IJ}$; 10-$EMIMDCA_{0.4\%}$, 11-$EMIMDCA_{9\%}$, 12-$EMIMDCA_{IJ}$; to make the analysis easier, the arrows indicate the glass transition temperatures of the IJs.

determined from DSC measurements is found for BPyDCAIJ being in the order of 3%.

The matrix rigidity causes a higher T_g for the IJs as earlier mentioned, an effect that is well illustrated in Figure 5 (indicated by an arrow).

Returning to the conductivity spectra, since the universal behavior is found for these systems with the plateau bending to a dispersive region as mentioned earlier, it is possible to simulate the real conductivity frequency dependence by the equation proposed by Jonscher:[41]

$$\sigma'(\omega) = \sigma_0\left[1 + \left(\frac{\omega}{\omega_{cross}}\right)^s\right] \quad (4)$$

where s $(0.5 \leq s \leq 1)$[42] is a material- and temperature-dependent parameter. The fit of eq 4 to the real conductivity allows σ_0 and ω_{cross} to be obtained from which the transport properties will be derived later on; the solid lines in Figure 4 are the obtained fits by the Jonscher law.

In Figure 6a–d, the dc conductivity (σ_0) values obtained from the fit of eq 4 are plotted against the temperature reciprocal for the 12 systems. In spite of some variations, it is obvious for all systems that the greater conductivity is exhibited by the bulk IL with 9% water. This is explained by a displacement of the counterions from the coordination shells by the lighter water molecules, weakening the electrostatic ion pair interactions.[43] This reduces caging and increases the diffusivity leading to a viscosity lowering and to an increase of charge transport mobility, conductivity, and diffusion coefficients.[44−46]

Due to the pronounced curvature exhibited in the σ_0 temperature dependence for all systems, the empirical VFTH equation was fitted to the conductivity data (eq 2b), which usually describes the temperature dependence of the structural relaxation time and the conductivity of supercooled liquids quite well.[47−50]

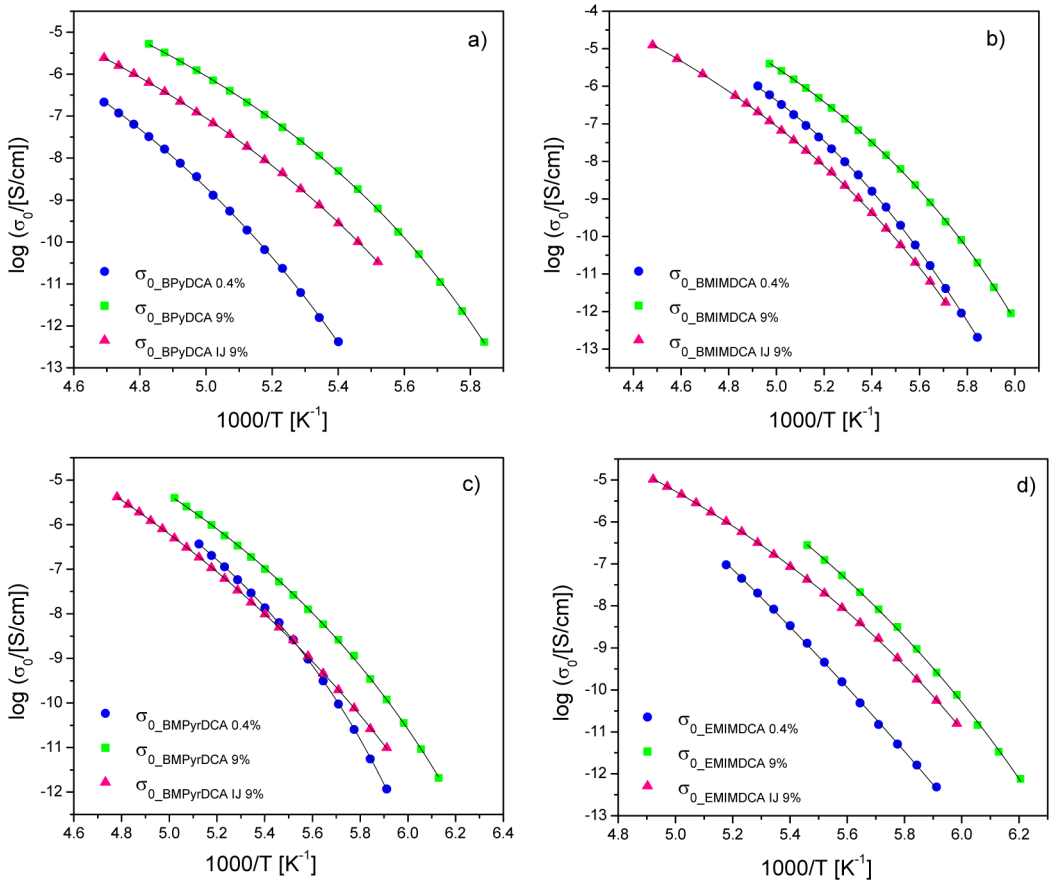

Figure 6. (a–d) Temperature dependence of the dc conductivity, σ_0, for all studied systems and for different hydrated states.

dx.doi.org/10.1021/jp502870q | J. Phys. Chem. B 2014, 118, 9445−9459

Table 3. Fit Parameters Obtained According to the VFTH Law for the σ_0 Conductivity (eq 2b)[a] and Fragility Index, m (eq 5)

sample	σ_∞/S·cm^{-1}	B/K	T_0/K	m
$BPyDCA_{0.4\%water}$	120.3 ± 26.3	1294 ± 26.7	140.7 ± 0.5	72
$BPyDCA_{9\%water}$	14.7 ± 2.8	1022.0 ± 19.6	138.5 ± 0.4	46
$BPyDCA_{Ion\ Jelly}$	36.6 ± 6.5	1307.3 ± 23.2	134.0 ± 0.5	33
$BMIMDCA_{0.4\%water}$	325 ± 115	1413 ± 46	131 ± 1	51
$BMIMDCA_{9\%water}$	68 ± 13	1176 ± 21	131 ± 0	48
$BMIMDCA_{Ion\ Jelly}$	67 ± 6	1469 ± 15	128 ± 0	48
$BMPyrDCA_{0.4\%water}$	20.5 ± 0.7	918.7 ± 27.9	136.7 ± 0.6	69
$BMPyrDCA_{9\%water}$	24.7 ± 7.7	1180.2 ± 40.4	123.7 ± 0.9	41
$BMPyrDCA_{Ion\ Jelly}$	276.3 ± 75.0	1721.8 ± 45.8	113.5 ± 0.9	33
$EMIMDCA_{0.4\%water}$	(7.9 ± 7.8)x10^{13}	5629.2 ± 1018.2	76.0 ± 9.3	48
$EMIMDCA_{9\%water}$	47611.3 ± 40162.8	1700.6 ± 197.4	117.3 ± 3.0	48
$EMIMDCA_{Ion\ Jelly}$	174.1 ± 41.8	1338.5 ± 32.5	122.6 ± 0.7	43

[a]The uncertainties are the statistical errors given by the fitting program.

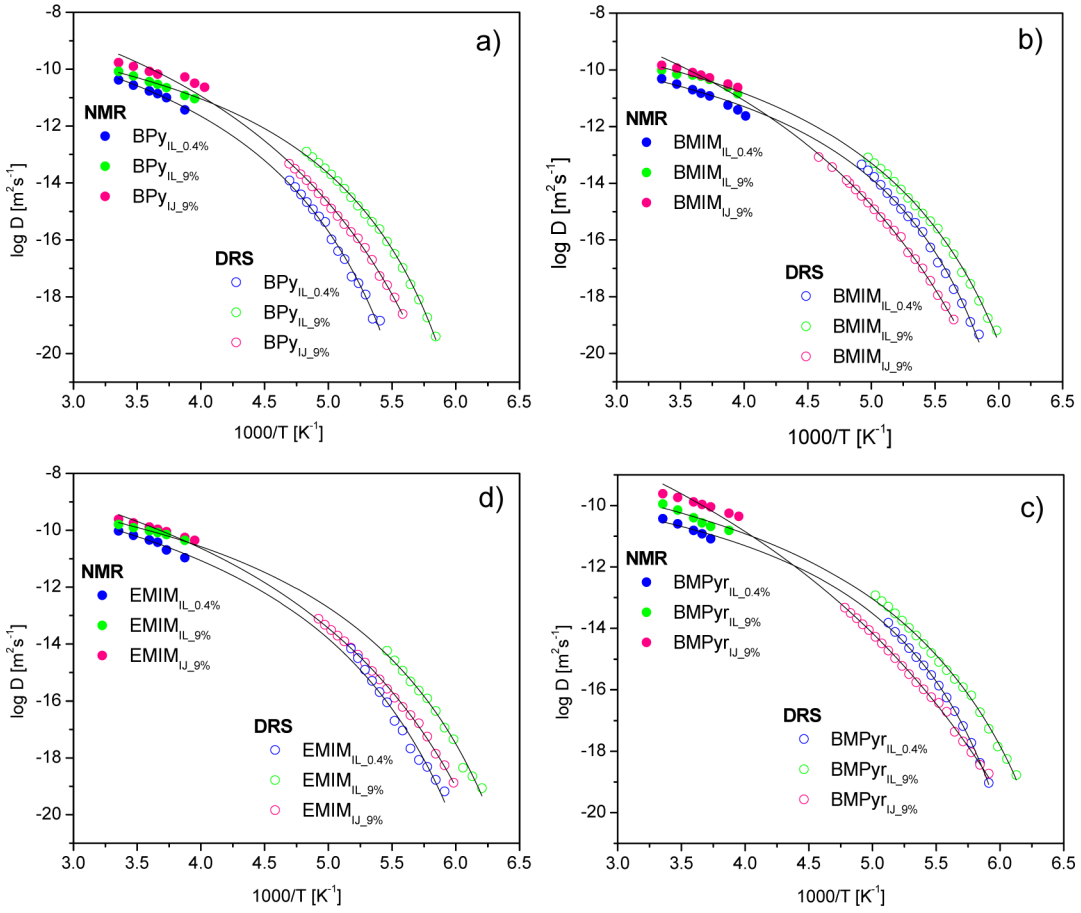

Figure 7. (a–d) Values of the cation diffusion coefficients (D_+) estimated from DRS data (eq 6a) and determined from PFG NMR; the VFTH fit is shown as solid lines.

The obtained VFTH fitting parameters of the conductivity temperature dependence are summarized in Table 3.

The curvature when conductivity is plotted against the temperature reciprocal (Figure 6) is associated with what is called a fragile behavior, as seen in many glass-forming substances,[51−54] quantified by the fragility index m expressed as[55]

$$m = \frac{BT_g}{\ln 10(T_g - T_0)^2} \quad (5)$$

with values typically range between m = 16 for strong systems and $m \approx 200$. Materials are called "strong" if their flow properties show a strong resistance when heated through their supercooled regime revealing a temperature dependence close to an Arrhenius-type behavior and "fragile" if the flow properties dramatically change in a narrow temperature range near the glass transition.[56] From the B parameter determined for $\sigma_0(1/T)$ and the calorimetric glass transition temperature, it is possible to estimate m through eq 5. The thus obtained m values are presented in Table 3 for all studied systems seeming that it falls closer in the category of strong materials and, in general, the IJs exhibit the lower fragilities there being an

dx.doi.org/10.1021/jp502870q | J. Phys. Chem. B 2014, 118, 9445−9459

Table 4. Fit Parameters Obtained According to the VFTH Law for the Diffusion Coefficient[a]

sample	D_∞/S·cm^{-1}	B/K	T_0/K
$BPyDCA_{0.4\%water}$	(2.6 ± 0.9)x10^{-8}	936.2 ± 57.7	149.9 ± 1.8
$BPyDCA_{9\%water}$	(8.4 ± 1.0)x10^{-9}	726.9 ± 16.6	143.5 ± 0.5
$BPyDCA_{Ion\ Jelly}$	(1.4 ± 0.7)x10^{-6}	1380.8 ± 101.9	132.2 ± 2.7
$BMIMDCA_{0.4\%water}$	(3.5 ± 0.9)x10^{-9}	692.9 ± 30.4	144.2 ± 1.0
$BMIMDCA_{9\%water}$	(1.8 ± 0.3) x10^{-8}	798.5 ± 24.8	137.5 ± 0.8
$BMIMDCA_{Ion\ Jelly}$	(2.6 ± 1.0) x10^{-6}	1572.5 ± 85.5	125.6 ± 2.2
$BMPyrDCA_{0.4\%water}$	(1.6 ± 0.2)x10^{-9}	620.9 ± 15.1	142.9 ± 0.6
$BMPyrDCA_{9\%water}$	(9.7 ± 2.0)x10^{-9}	792.1 ± 30.3	131.6 ± 1.0
$BMPyrDCA_{Ion\ Jelly}$	(2.0 ± 0.9)x10^{-5}	2024.8 ± 123.8	107.0 ± 2.9
$EMIMDCA_{0.4\%water}$	(3.2 ± 2.0)x10^{-8}	942.7 ± 89.0	135.2 ± 2.8
$EMIMDCA_{9\%water}$	(2.4 ± 0.6)x10^{-8}	805.6 ± 41.0	131.3 ± 1.4
$EMIMDCA_{Ion\ Jelly}$	(4.2 ± 0.9)x10^{-7}	1229.4 ± 37.3	124.4 ± 1.1

[a]The uncertainties are the statistical errors given by the fitting program.

additional parameter that reveals their higher stability against thermal treatment.

In a previous publication by some of us,[21] the overall diffusion coefficient was decomposed into its cationic (D_+) and anionic (D_-) contributions as

$$D_+ = \frac{\langle \Delta r_+^2(t^*) \rangle}{6\gamma} \nu_{cross} \quad (6a)$$

and

$$D_- = \frac{\langle \Delta r_-^2(t^*) \rangle}{6\gamma} \nu_{cross} \quad (6b)$$

where $\langle \Delta r_+^2(t^*) \rangle$ and $\langle \Delta r_-^2(t^*) \rangle$ are the mean-square displacements for the cation and anion, respectively, estimated by taking the square of the van der Waals (vdW) diameter (see vdW radius in the Experimental Section); $\gamma \approx 2$ is a numerical factor reflecting the conductivity spectrum at the onset of ac conduction.

Figure 7 presents the temperature dependence of the cation diffusion coefficients estimated from eq 6a). Included are the respective values directly measured by pulsed filed gradient NMR revealing very good agreement, thus validating the DRS data treatment.

Because of the absence of protons or highly sensitive NMR nuclei in the DCA anion structure, its diffusion coefficients were not able to be determined by NMR.

By combining the results of both techniques it is possible to access the diffusion coefficients over a broad temperature range ($\Delta T \approx 150$ K), within which D values vary around 10 decades. Close to room temperature, the D values for the bulk ILs are in agreement with the ones found for a series of ionic liquids, varying between 10^{-10} and 10^{-11} m^2·s^{-1}.[57−59] The highest values for both conductivity ~10^{-2} S·cm^{-1} and diffusion coefficient ~10^{-10} m^2·s^{-1} at room temperature were found for the ion jelly derived from EMIMDCA.

The temperature dependence of the IL diffusion coefficients with the two water contents obeys a VFTH as found for conductivity; respective parameters are presented in Table 4. As observed before for conductivity, the highest D values at low temperatures (160 to 210 K) are found for the most hydrated IL. Interestingly, the behavior changes at the highest temperatures: while bulk ILs follow a more or less smooth VFTH curve, the temperature dependence for D_{IJ} changes significantly close to room temperature (258 to 308 K), and the diffusion coefficients become comparable or even higher than those for $IL_{9\%}$. This seems to indicate some kind of transition of the gelatin matrix between the two temperature ranges, being very rigid at low temperatures hindering the diffusion of the incorporated IL and much less viscous at room temperature facilitating the IL mass flux. In fact, an endothermic transition with onset just above 293 K and centered close to 316 K is reported for wet un-cross-linked gelatin assigned to helix−coil transition of gelatin on undergoing denaturation.[60] The detection of such a thermal event was not possible for any of the IJs nor for hydrated gelatin (22% w/w water) due to the broad endotherm associated with water evaporation (remember the DSC thermogram for hydrated $BMIMDCA_{IJ}$ (1st scan) in Figure 3).

The diffusion coefficient, associated with mass transport, is higher at high temperatures in IJs, meaning that mass transport is occurring over a less resistant medium relative to bulk IL. This is coherent with the absence of specific interactions between the gelatin matrix and the IL cation/anion while in the less hydrated ILs, cation−anion interactions dominate being partially replaced by cation−water and anion−water interactions in the most hydrated IL. This and the fluidity of hydrated gelatin at those temperatures due to hydrogen bonds breaking facilitates the mass transport.

The temperature dependence for diffusion coefficients differs from the one obeyed by conductivity for all the IJs, pointing to a difference between mass and charge transport. The analysis at room temperature of those quantities for one of the systems, BPyDCA, is done in Figure 8.

While the diffusion coefficient increases with the water content increase for the bulk IL and increases even more for the IJ having the same water content than the bulk IL (9%), the conductivity increases as expected with the increase of hydration, but decreases for the IJ. This gives further evidence that water in the IJ is not in all extents interacting/solvating the IL cations and anions, since as already mentioned, it is assuring the gelatin structure. The decrease of conductivity for the IJ is due to a smaller amount of ionic species (lower content of IL) since gelatin itself poorly contributes for conductivity; even with 22% of hydration the conductivity of gelatin in 4 to 8 decades is inferior to IJ.[21]

Type of Interaction. The T_0 values obtained from the conductivity temperature dependence together with the glass transition temperature are frequently used to establish a correlation with structural properties as the size of the ILs cation/anion, molecular volume or length of the alkyl

dx.doi.org/10.1021/jp502870q | J. Phys. Chem. B 2014, 118, 9445−9459

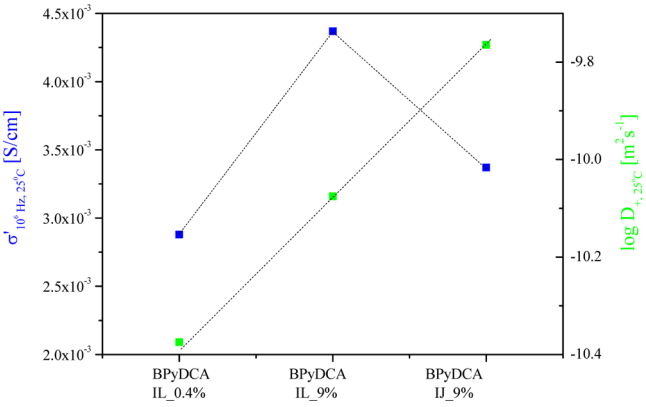

Figure 8. Conductivity and cation diffusion coefficient of BPyDCA for different water contents in bulk and entrapped in the ion jelly, illustrating the difference between charge (σ) and mass (D) transport (lines are guides for the eyes).

chain,[50,61,62] also σ_∞ was correlated with the species size, either anion[48,63] or cation.[50,63]

This kind of analysis is impractical for the tested ILs since the change in radius and volume is almost negligible; from the smallest ionic cation, EMIM, to the largest, BPy, the radius changes less than 1 Å (see the Experimental Section). An alternative discussion could be done based in the dependence of the glass transition on the type of interionic cohesive forces:[38,47,64] (i) attractive Coulombic forces that dominate for low molecular volumes (<250 cm^3/mol) for which T_g significantly decreases with increasing molar volume, and (ii) van der Waals forces that dominate if the molar volume is large (>250 cm^3/mol), which lead to an increase of T_g with increasing molar volume or cation radius;[47] a broad minimum in the ionic liquid cohesive energy occurs at a molar volume of 250 cm^3·mol^{-1} as depicted in Figure 9 (adapted from ref 64). The tested ILs have *molecular* volumes from 184.5 to 214.5

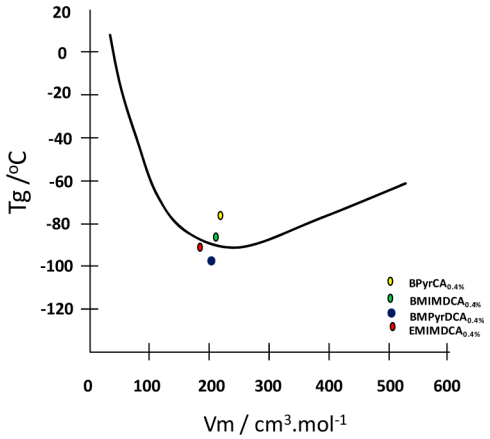

Figure 9. Insertion of T_g (V_m) data determined in the present work in the plot provided in ref 64 (here adapted) representing the dependence of the cohesion of salts of weakly polarizable cations and anions, assessed by the T_g value, on the ambient temperature molar volume, V_m, and, hence, on the interionic spacing $[(r^+ + r^-) \approx V_m^{1/3}]$. A broad minimum in the ionic liquid cohesive energy is seen at a molar volume of 250 cm^3 mol^{-1}, which corresponds to an interionic separation of ~0.6 nm, assuming a face-centered-cubic packing of anions about the cations. The line through the points is a guide to the eye.

cm^3·mol (see Experimental Section), falling close to the critical *molecular* volume that corresponds to the lower T_g values of the proposed correlation, revealing relatively good agreement to what is predicted (filled circles in Figure 9). While small ionic salts such as $LiNO_3$ and $LiClO_3$ have some of the highest T_g values (10 and −20 °C, respectively), the lower glass transition temperatures (below −80 °C) are found for the ILs $MOMNM_2E^+$, $EOMNM_2E^+$, $MOENM_2E^+$, BF_4^-, $TFSI^-$, and TF^-.[64] The found dependence of the cohesion assessed by the T_g value for the ILs under study in this work is identical with the one followed for those ILs. This is due to a counterbalance between Coulombic and van der Waals interactions in the ILs under study.

Dipolar Relaxation. As previously mentioned, for the dielectric response of a material not only charge transport processes contribute as was mainly analyzed in this work, but also interfacial polarizations and reorientational motions of dipoles. The latter give rise to relaxational processes, which spectrally manifest as a peak in the imaginary part of permittivity ε'' and a sigmoidal curve in the real part ε' of the complex dielectric function against frequency. This was clearly found for $BMPyrDCA_{0.4\%}$ as shown in Figure 10: the

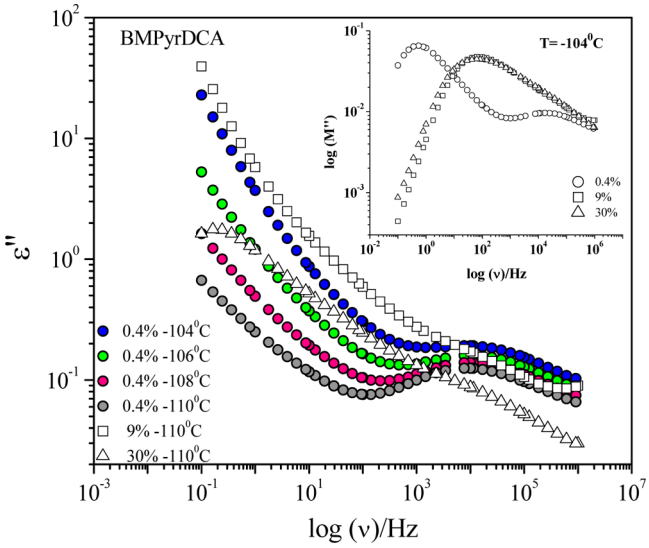

Figure 10. Imaginary part of the complex dielectric function for the secondary relaxation process in $BMPyrDCA_{0.4\%}$ at subglass temperatures; the respective plots at −110 °C for the same IL with 9% and 30% water content were included. The inset depicts the imaginary part of the modulus for the three systems at −104 °C.

conductivity contribution at lower temperatures is relatively small and the imaginary part of the complex permittivity, ε'', exhibits a well-defined peak, which shifts to higher frequencies as a consequence of the mobility enhancement driven by the temperature increasing. The $\varepsilon''(\nu)$ curves depicted in Figure 10 were collected at temperatures below the calorimetric glass transition of $BMPyrDCA_{0.4\%}$. Therefore, the relaxation process seems to be compatible with a secondary one, as detected in molecular glass formers but also in ionic liquids.[65] To analyze in more detail the origin of this process, mainly if it could be related to the presence of water, the corresponding plots for $BMPyrDCA_{9\%}$ and for an even more hydrated sample, $BMPyrDCA_{30\%}$, were compared; see the respective $\varepsilon''(\nu)$ curves included in Figure 10 at −110 °C. The increase of hydration does not reflect in an enhancement of the dielectric

dx.doi.org/10.1021/jp502870q | J. Phys. Chem. B 2014, 118, 9445−9459

response, which seems to pull apart the reorientational motion of water molecules as being in its origin, as reported e.g., in ref 66. Furthermore, all the curves exhibit a low frequency tail that increases significantly with the temperature increase, denouncing the arrival of the relaxation process associated with the dynamical glass transition involving larger scale motions. To allow the characterization of this incoming process, since it is highly masked by conductivity, it is more convenient to carry on its analysis based on the complex electric modulus (M^*) formalism,[67,68] which is defined as the reciprocal of the complex permittivity $M^*(\omega) = 1/\varepsilon^*(\omega)$.[69−71]

The imaginary part of the complex electric modulus, $M^*(\omega) = M'(\omega) + iM''(\omega)$ is depicted in the inset of Figure 10 at −104 °C for each of the BMPyrDCA hydration levels and will be analyzed with an equivalent of the HN equation (eq 1) given by[20]

$$M^*(\omega) = M_\infty + \frac{\Delta M}{(1 + (-1(\omega\tau_{HN-M})^{-1})^{\beta_{HN}})^{\gamma_{HN}}} \quad (7)$$

which is widely used to suppress conductivity and polarization phenomena and to reveal the dipolar contributions.[72]

The relaxation times extracted after the fitting of eq 7 to M'' and those obtained after simulation by the HN function (eq 1) were converted to a model-independent relaxation time, $\tau_{max} = 1/(2\pi\nu_{max})$, according to[20]

$$\tau = \tau_{HN}\left[\frac{\sin\left(\frac{\alpha_{HN}\beta_{HN}\pi}{2+2\beta_{HN}}\right)}{\sin\left(\frac{\alpha_{HN}\pi}{2+2\beta_{HN}}\right)}\right]^{1/\alpha_{HN}} \quad (8)$$

where τ_{HN}, α_{HN}, and β_{HN} are the parameters obtained from eq 1.

The thus obtained values are depicted in Figure 11. The simulation by eq1 was only possible for the secondary relaxation of the three systems and the α-process of BMPyrDCA$_{30\%}$. An additional process due to conductivity was also detected and submitted to the same data treatment according eqs 7 and 8. It is obvious the curvature of the conductivity and dipolar response of the α-process obeys a VFTH law (see parameters in Table 5). From the extrapolation of the ε'' relaxation times to τ = 100 s,[55,73] a glass transition temperature is estimated ($T_{g,Diel}$) as 157.8 K to BMPyrDCA$_{30\%}$. The same extrapolation for the M'' relaxation times gives a $T_{g,M''}$ = 156.9 K, so it seems to be valid to extend this procedure to BMPyrDCA$_{9\%}$ and BMPyrDCA$_{0.4\%}$ to have a rough estimate of the glass transition temperatures (see values in Table 5). This approach allows the glass transition temperature for the less hydrated system to be distinguished, while both 9% and 30% give very similar T_g values pointing to a saturation of the IL for water contents ≤9%. The higher value for the less hydrated sample (∼9 K above T_g of either BMPyrDCA$_{9\%}$ or BMPyrDCA$_{30\%}$) made possible the better resolution of the secondary relaxation in BMPyrDCA$_{0.4\%}$ since the α-process is shifted to lower frequencies in the spectral window.

The traces that define the relaxation times of the secondary processes are linear and highly superimpose at the lowest temperatures. This acts as a further confirmation that the observed relaxation process is different from the one detected in aqueous binary solutions of several glass-formers[66,74,75] which shift to higher frequencies/lower temperatures with the water content increase.

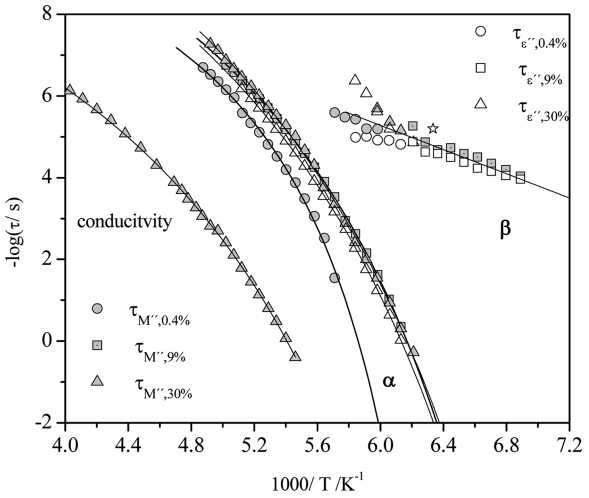

Figure 11. Relaxation map for BMPyrDCA$_{0.4\%}$, BMPyrDCA$_{9\%}$, and BMPyrDCA$_{30\%}$ where the relaxation times were obtained by the fit of eq 6a,b to the imaginary part of the complex modulus; the activation plots of the imaginary part of the complex permittivity were included when the fit was possible. The lines are fits of the VFTH (eq 2a) and Arrhenius equation to the corresponding data; the latter was estimated based on the relaxation times of the secondary relaxation found for 9% and 30%, which have similar glass transition temperatures. The star indicates the relaxation time obtained by the coupling model (eq 9), using the shape parameters estimated in the simulation of the ε'' for the α-process of BMPyrDCA$_{30\%}$.

Nevertheless for samples with 9% but mainly 30% water, the traces of the secondary process bent off while crossing T_g. This is observed for the temperature dependence of the Johari−Goldstein process taken as the precursor of the relaxation process responsible for the dynamical glass transition in the framework of the Coupling Model (CM).[76] To confirm this attribution the relaxation time of the detected β-process must be close to the one predicted by the CM model for the JG process, $\tau_{\beta JG}$, through the equation:

$$\tau_{JG}(T) \approx \tau_0(T) = \tau_c^{\,n}[\tau_\alpha(T)]^{1-n} \quad (9)$$

where τ_0 is the primitive relaxation time of the CM, n is the coupling parameter, τ_c is a time characterizing the crossover from independent to cooperative fluctuations found to be close to 2×10^{-12} s for molecular glass formers,[77] $\tau_\alpha = \tau_{KWW}$ is the relaxation time of the Kohlrausch−Williams−Watts (KWW) function,[78−80] and $\varphi(t) = \exp[-(t/\tau_{KWW})^{\beta_{KWW}}]$ describes the relaxation response in the time domain; $0 < \beta_{KWW} < 1$; $\beta_{KWW} = 1$ for a Debye response. The β_{KWW} parameter can be estimated through the HN shape parameters of the α-process by using the empirical correlation ($\beta_{KWW} = (\alpha_{HN}\beta_{HN})^{1/1.23}$) proposed by Alegria et al.[81] This can be tested for BMPyrDCA$_{30\%}$, for which eq 1 was fitted to ε'' data, giving α_{HN} = 0.8 and β_{HN} = 0.5 as fit shape parameters, allowing a value of β_{KWW} = 0.47 to be obtained. The coupling parameter, n, is equal to $1 - \beta_{KWW}$, giving at $T_{g,Diel}$ a value of $\tau_{JG} \approx \tau_0 = 6.4 \times 10^{-6}$ s. This value is in agreement with the experimental τ_β value at 157.8 K ($T_{g,Diel}$) as indicated by the star in the relaxation map of Figure 11, which seems to confirm the assignment to a Johari−Goldstein β relaxation (β_{JG}). Moreover, this attribution can be confirmed by testing the ratio $E_{a,\beta}/RT_g$, where $E_{a,\beta}$ is the glassy state activation energy of the β_{JG}-process, T_g is the glass transition temperature of the α relaxation, and R is the gas constant, if the temperature dependence of relaxation times for the secondary

dx.doi.org/10.1021/jp502870q | J. Phys. Chem. B 2014, 118, 9445−9459

Table 5. Estimated Parameters of the Fit of the VFTH Law (eq 2a) to the Temperature Dependence of Relaxation Times of the α-Process Obtained from the Analysis of the Electric Modulus (M'')[a]

	BMPyrDCA sample				
VFTH parameters	$M''_{0.4\%}$	$M''_{9\%}$	$M''_{30\%}$	$\varepsilon''_{30\%}$	conductivity$_{30\%}$
τ_∞/s	3.9×10^{-12}	1.9×10^{-14}	2.9×10^{-16}	2.4×10^{-15}	4.4×10^{-12}
B/K	647.8	1201.6	1647.9	1478.5	1416.0
T_0/K	146.0	124.1	116.0	119.2	130.8
T_g/K (τ = 100 s)	167.0	157.3	156.9	157.8	

[a]For the 30% sample, the fit parameters of the complex permittivity (ε'') and conductivity are included. The glass transition temperatures were estimated by extrapolating the VFTH equation to τ = 100 s.

relaxation is described by an Arrhenius law: $\tau(T) = \tau_\infty \exp(E_a/RT)$; τ_∞ is the pre-exponential factor. The activation energy thus determined taking into account data before the strong bending of BMPyrDCA with 9% and 30%, which have similar glass transition temperatures, is 28.4 kJ mol^{-1}. This gives a $E_{a,\beta}/RT_g$ ratio of 22 close to E_a/RT_g = 24 as proposed by Kudlik et al.[82] found for several glass formers[83] and also for ionic liquids;[84] the respective prefactor is 7×10^{-15} s, agreeing with the τ_∞ values usually found for the JG process.

The observation of dipolar relaxation means that under the influence of the external electrical field the IL under testing behaves mainly as a single ionic dipole instead of separated anion and cation.

The diffusion coefficients were estimated well above the glass transition, i.e., at a temperature at which the conductivity overwhelms the dipolar contribution.

The type of mobility that sets in with the temperature increase while crossing the glass transition enables the translational motion of charge carriers, increasing conductivity and masking the relaxation processes, i.e., the number of species that behave as a separate cation−anion pair start to dominate over those that respond to the applied filed as a single ionic dipole.

CONCLUSION

Several physicochemical properties of dicianamide (DCA) ionic liquids (ILs) with different hydration levels and respective ion jellies (IJs) were investigated by means of differential scanning calorimetry (DSC), dielectric relaxation spectroscopy (DRS), and pulse field gradient nuclear magnetic resonance (PFG NMR). In particular, the temperature-driven physical transformations, glass transition temperature, conductivity, diffusion, and fragility of ILs and IJs were evaluated.

By DSC it was shown that all the studied systems are glass formers since they all exhibit a glass transition. A significant increase on the glass transition temperature (T_g) upon dehydration was observed for all materials, with a higher extent for the IJs. The higher T_g for the IJs was interpreted, for the hydrated systems, as water being partionated between the IL and gelatin solvating to a less extent the IL compared with bulk for the same water content (9%); after water removal, the higher T_g for the IJ could be an effect of hindered IL mobility over a relatively stiff dehydrated gelatin matrix. Moreover, upon water removal with the exception of BPyDCA, all the other ILs are crystallizable. Crystallization was never observed for any IJ meaning that the entrapment in gelatin provides stability against crystallization.

The real conductivity, σ', was measured for all systems. A correlation between the temperature at which a plateau emerges in the frequency dependence conductivity plot, due to long-range motion of charge carriers (diffusive regime), and the onset of structural relaxation which is in the origin of the glass transition seems to exist. While for the IJs and hydrated ILs the emergence of a plateau in the $\sigma'(\nu)$ plot occurs very near the temperature onset of the calorimetric glass transition, for the less hydrated ILs the diffusive regime is established later on, surpassing the glass transition, which may indicate that some additional energy must be provided to overpass interionic interactions. In the hydrated ILs the conductivity is higher since water facilitates the translational motion of charge carriers. In all systems, the conductivity decreases significantly with the temperature decrease obeying a Volger−Fulcher−Tamman−Hess law giving rise to a curved plot allowing the fragility index to be estimated. Although there are no significant variations between the different systems, the IJ are less fragile which indicates a more resistant behavior against thermal treatment. A curvature is also found in the temperature dependence of the diffusion coefficients extracted at the lowest temperatures from conductivity measurements showing a good agreement with the PFG NMR measurements carried out at temperatures close to ambient. The combination of data estimated from the two techniques allows a temperature range of about 150 K to be covered over which the cation diffusion coefficients vary more than 10 decades. Interestingly, a difference between charge and mass transport was found for the IJ systems. While conductivity increases with the hydration as expected for the bulk IL, in the IJ with the same water content it decreases, due to a lower number of charge carriers since by one side water is involved in H-bonds assuring the gelatin structure and by other less IL is incorporated in the composite relative to bulk ionic liquid. The IJs diffusion coefficients being lower than the IL with the same water content at low temperatures become comparable to the IL$_{9\%}$ or even higher (EMIMDCA) at room temperature which points to some structural change in the gelatin matrix as helical-coil transition favoring mass transport. This seems to indicate that no specific interactions between IL ions and gelatin constituent occur.

The IJ derived from EMIMDCA besides exhibiting the higher diffusion coefficient at temperatures close to ambient also exhibits the highest conductivity. This result opens new doorways toward the design of novel ILs that could even improve this phenomenon.

Furthermore, for BMPyrDCA the dipolar response was analyzed through both permittivity and modulus formalisms allowing assigning the subglass response to a Johari−Goldstein process as observed in molecular glass formers.

AUTHOR INFORMATION

Corresponding Author

*E-mail: madalena.dionisio@fct.unl.pt.

Notes

The authors declare no competing financial interest.

■ ACKNOWLEDGMENTS

M.D. acknowledges the helpful discussions with J. C. Lima (Requimte FCT/UNL) and J. J. Moura Ramos (IST/UTL). Financial support by Fundação para a Ciência e a Tecnologia (FCT/MEC) through projects PEst-C/EQB/LA0006/2011, PTDC/EBB-EBI/099237/2008, and PTDC/CTM/100244/2008 and by FEDER is acknowledged. T.C. and P.V. acknowledge, respectively, the PhD grant SFRH/BD/47088/2008 and the Postdoc grant SFRH/BPD/41546/2007. The NMR spectrometers are part of the National NMR Network (RNRMN) and are funded by Fundação para a Ciência e Tecnologia (project RECI/BBB-BQB/0230/2012).

■ REFERENCES

(1) Galiński, M.; Lewandowski, A.; Stępniak, I. Ionic Liquids as Electrolytes. *Electrochim. Acta* **2006**, *51*, 5567−5580.
(2) Fernicola, A.; Scrosati, B.; Ohno, H. Potentialities of Ionic Liquids as New Electrolyte Media in Advanced Electrochemical Devices. *Ionics* **2006**, *12*, 95−102.
(3) Lu, W.; Fadeev, A. G.; Qi, B.; Smela, E.; Mattes, B. R.; Ding, J.; Spinks, G. M.; Mazurkiewicz, J.; Zhou, D.; Wallace, G. G.; MacFarlane, D. R.; Forsyth, S. A.; Forsyth, M. Use of Ionic Liquids for π-Conjugated Polymer Electrochemical Devices. *Science* **2002**, *297*, 983−987.
(4) Yoshida, Y.; Baba, O.; Saito, G. Ionic Liquids Based on Dicyanamide Anion: Influence of Structural Variations in Cationic Structures on Ionic Conductivity. *J. Phys. Chem. B* **2007**, *111*, 4742−4749.
(5) Torimoto, T.; Tsuda, T.; Okazaki, K.; Kuwabata, S. New Frontiers in Materials Science Opened by Ionic Liquids. *Adv. Mater.* **2010**, *22*, 1196−1221.
(6) Delaney, J. T.; Liberski, A. R.; Perelaer, J.; Schubert, U. S. A Practical Approach to the Development of Inkjet Printable Functional Ionogels-Bendable, Foldable, Transparent, and Conductive Electrode Materials. *Macromol. Rapid Commun.* **2010**, *31*, 1970−1976.
(7) Carvalho, T.; Vidinha, P.; Vieira, B. R.; Li, R. W. C.; Gruber, J. Ion Jelly: a Novel Sensing Material for Gas Sensors and Electronic Noses. *J. Mater. Chem. C* **2014**, *2*, 696−701.
(8) Dobler, D.; Schmidts, T.; Klingenhöfer, I.; Runkel, F. Ionic liquids as Ingredients in Topical Drug Delivery Systems. *Int. J. Pharm.* **2013**, *441*, 620−627.
(9) He, Y.; Boswell, P. G.; Bühlmann, P.; Lodge, T. P. Ion Gels by Self-Assembly of a Triblock Copolymer in an Ionic Liquid. *J. Phys. Chem. B* **2007**, *111*, 4645−4652.
(10) Le Bideau, J.; Viau, L.; Vioux, A. Ionogels, Ionic Liquid based Hybrid Materials. *Chem. Soc. Rev.* **2011**, *40*, 907−925.
(11) Tiyapiboonchaiya, C.; Pringle, J. M.; MacFarlane, D. R.; Forsyth, M.; Sun, J. Polyelectrolyte in Ionic Liquid Electrolytes. *Macromol. Chem. Phys.* **2003**, *204*, 2147−2154.
(12) Jiang, J.; Gao, D.; Li, Z.; Su, G. Gel Polymer Electrolytes Prepared by in situ Polymerization of Vinyl Monomers in Room-Temperature Ionic Liquids. *React. Funct. Polym.* **2006**, *66*, 1141−1148.
(13) Ohno, H.; Yoshizawa, M.; Ogihara, W. Development of New Class of Ion Conductive Polymers Based on Ionic Liquids. *Electrochim. Acta* **2004**, *50*, 255−261.
(14) Washiro, S.; Yoshizawa, M.; Nakajima, H.; Ohno, H. Highly Ion Conductive Flexible Films Composed of Network Polymers Based on Polymerizable Iionic Liquids. *Polymer* **2004**, *45*, 1577−1582.
(15) Winther-Jensen, O.; Vijayaraghavan, R.; Sun, J.; Winther-Jensen, B.; MacFarlane, D. R. Self Polymerising Ionic Liquid Gel. *Chem. Commun.* **2009**, *21*, 3041−3043.
(16) Vidinha, P.; Lourenço, N. M. T.; Pinheiro, C.; Brás, A. R.; Carvalho, T.; Santos-Silva, T.; Mukhopadhyay, A.; Romão, M. J.; Parola, J.; Dionisio, M.; Cabral, J. M. S.; Afonso, C. A. M.; Barreiros, S. Ion jelly: a Tailor-Made Conducting Material for Smart Electrochemical Devices. *Chem. Commun.* **2008**, *44*, 5842−5844.
(17) Couto, R. M.; Carvalho, T.; Neves, L. A.; Ruivo, R. M.; Vidinha, P.; Paiva, A.; Coelhoso, I. M.; Barreiros, S.; Simões, P. C. Development of Ion-Jelly® Membranes. *Sep. Purif. Technol.* **2013**, *106*, 22−31.
(18) Pimenta, A. F. R.; Baptista, A. C.; Carvalho, T.; Brogueira, P.; Lourenço, N. M. T.; Afonso, C. A. M; Barreiros, S.; Vidinha, P.; Borges, J. P. Electrospinning of Ion Jelly Fibers. *Mater. Lett.* **2012**, *83*, 161−164.
(19) Rana, S.; Carvalho, T.; Fangueiro, R.; Vidinha, P. Silk-Ion Jelly: a Novel Ion Conducting Polymeric Material with High Conductivity and Excellent Mechanical Stability. *Polym. Adv. Technol.* **2013**, *24*, 191−196.
(20) Schönhals, A.; Kremer, F. *Analysis of Dielectric Spectra in Broadband Dielectric Spectroscopy*; Schönhals, A., Kremer, F., Eds.; Springer-Verlag: Berlin Germany, 2003; Chapter 3.
(21) Carvalho, T.; Augusto, V.; Brás, A. R.; Lourenço, N. M. T.; Afonso, C. A. M.; Barreiros, S.; Correia, N. T.; Vidinha, P.; Cabrita, E. J.; Dias, C. J.; Dionísio, M.; Roling, B. Understanding the Ion Jelly Conductivity Mechanism. *J. Phys. Chem. B* **2012**, *116*, 2664−2676.
(22) Triolo, A.; Russina, O.; Bleif, H. J.; Di Cola, E. Nanoscale Segregation in Room Temperature Ionic Liquids. *J. Phys. Chem. B* **2007**, *111*, 4641−4644.
(23) Steeman, P. A. M.; van Turnhout, J. *Dielectric Properties of Inhomogeneous Mediain Broadband Dielectric Spectroscopy*; Kremer, F., Schönhals, A., Eds.; Springer-Verlag: Berlin, Germany, 2003; Chapter 13.
(24) Fredlake, C. P.; Crosthwaite, J. M.; Hert, D. G.; Aki, S. N. V. K.; Brennecke, J. F. Thermophysical Properties of Imidazolium-Based Ionic Liquids. *J. Chem. Eng. Data* **2004**, *49*, 954−964.
(25) González, E. J.; Begona, G.; Macedo, E. A. Thermophysical Properties of the Pure Ionic Liquid 1-Butyl-1-methylpyrrolidinium Dicyanamide and Its Binary Mixtures with Alcohols. *J. Chem. Eng. Data* **2013**, *58*, 1441−1448.
(26) Spartan Student, V4.1.2; Wavefunction Inc.: Irvine, CA.
(27) Menczel, J. D.; Prime, R. B. *Thermal Analysis of Polymers in Fundamentals and Applications*; John Wiley: Hoboken, NJ, 2009.
(28) Havriliak, S.; Negami, S. A complex Plane Analysis of alpha-dispersion in Some Polymer Systems. *J. Polym. Sci.* **1966**, *14PC*, 99.
(29) Havriliak, S.; Negami, S. A Complex Plane Representation of Processes in Some Polymers. *Polymer* **1967**, *8*, 16.
(30) Fulcher, G. S. Analysis of Recent Measurements of the Viscosity of Glasses. *J. Am. Ceram. Soc.* **1925**, *8*, 339−355.
(31) Vogel, H. The Temperature Dependence Law of the Viscosity of Fluids. *Phys. Z.* **1921**, *22*, 645−646.
(32) Tammann, G.; Hesse, W. The dependancy of viscosity on temperature in hypothermic liquids. *Z. Anorg. Allg. Chem.* **1925**, *156*, 245−257.
(33) Dionisio, M.; Mano, J. F. *Electrical Techniques in Handbook of Thermal Analysis and Calorimetry*, 5th ed.; Elsevier: New York, NY, 2008; pp 209−268.
(34) Wu, D.; Chen, A.; Johnson, C. S., Jr. An Improved Diffusion-Ordered Spectroscopy Experiment Incorporating Bipolar-Gradient Pulses. *J. Magn. Reson.* **1995**, *A115*, 260−264.
(35) Troshenkova, S. V.; Sashina, E. S.; Novoselov, N. P.; Arndt, K. F.; Jankowsky, S. Structure of Ionic Liquids on the Basis of Imidazole and their Mixtures with Water. *Russ. J. Gen. Chem.* **2010**, *80*, 106−111.
(36) Huddleston, J. G.; Visser, A. E.; Reichert, W. M.; Willauer, H. D.; Broker, G. A.; Rogers, R. D. Characterization and Comparison of Hydrophilic and Hydrophobic Room Temperature Ionic Liquids Incorporating the Imidazolium Cation. *Green Chem.* **2001**, *3*, 156−164.
(37) Konig, A.; Stepanskib, M.; Kuszlikb, A.; Keila, P.; Weller, C. Ultra-purification of ionic liquids by melt crystallization. *Chem. Eng. Res. Des.* **2008**, *86*, 775−780.
(38) Sangoro, J. R.; Iacob, C.; Naumov, S.; Valiullin, R.; Rexhausen, H.; Hunger, J.; Buchner, R.; Strehmel, V.; Kärger, J.; Kremer, F. Diffusion in Ionic Liquids: the Interplay Between Molecular Structure and Dynamics. *Soft Matter* **2011**, *7*, 1678.

(39) Dyre, J. C.; Jacobsen, J. M. Universal Time Dependence of the Mean-Square Displacement in Extremely Rugged Energy Landscapes with Equal Minima. *Phys. Rev. B* **1995**, *52*, 2429−2433.
(40) Roling, B. Charge Transport in Disordered Solids with Applications in Electronics. In *Mechanisms of Ion Transport in Amorphous and Nanostructured Materials*; John Wiley: New York, NY, 2006; p 382.
(41) Jonscher, A. K. Universal Dielectric Response. *Nature* **1977**, *267*, 673−679.
(42) Schönhals, A.; Kremer, F. *Analysis of Dielectric Spectra in Broadband Dielectric Spectroscopy*; Schönhals, A., Kremer, F., Eds.; Springer-Verlag: Berlin, Germany, 2003; Chapter 12.
(43) Spohr, H. V.; Patey, G. N. The Influence of Water on the Structural and Transport Properties of Model Ionic Liquids. *J. Chem. Phys.* **2010**, *132*, 234510.
(44) Kohno, Y.; Ohno, H. Ionic Liquid/Water Mixtures: from Hostility to Conciliation. *Chem. Commun.* **2012**, *48*, 7119−7130.
(45) Huddleston, J. G.; Visser, A. E.; Reichert, W. M.; Willauer, H. D.; Broker, G. A.; Rogers, R. D. Characterization and Comparison of Hydrophilic and Hydrophobic Room Temperature Ionic Lliquids Incorporating the Imidazolium Cation. *Green Chem.* **2001**, *3*, 156−164.
(46) Chang, T. M.; Dang, L. X.; Devanathan, R.; Dupuis, M. Structure and dynamics of N,N-diethyl-N-methylammonium triflate Ionic Liquid, Neat and with Water, from Molecular Dynamics Simulations. *J. Phys. Chem. A* **2010**, *114*, 12764−12774.
(47) Leys, J.; Wübbenhorst, M.; Preethy Menon, C.; Rajesh, R.; Thoen, J.; Glorieux, C.; Nockemann, P.; Thijs, B.; Binnemans, K.; Longuemart, S. Temperature Dependence of the Electrical Conductivity of Imidazolium Iionic Liquids. *J. Chem. Phys.* **2008**, *128*, 064509.
(48) Zech, O.; Stoppa, A.; Buchner, R.; Kunz, W. The Conductivity of Imidazolium-Based Ionic Liquids from (248 to 468) K. Variation of the Anion. *J. Chem. Eng. Data* **2010**, *55*, 1774−1778.
(49) Ito, N.; Huang, W.; Richert, R. Dynamics of a Supercooled Ionic Liquid Studied by Optical and Dielectric Spectroscopy. *J. Phys. Chem. B* **2006**, *110*, 4371−4377.
(50) Iacob, C.; Sangoro, J. R.; Serghei, A.; Naumov, S.; Korth, Y.; Kärger, J.; Friedrich, C.; Kremer, F. Charge Transport and Glassy Dynamics in Imidazole-Based Liquids. *J. Chem. Phys.* **2008**, *129*, 234511 1−5.
(51) Leys, J.; Rajesh, R. N.; Menon, P. C.; Glorieux, C.; Longuemart, S.; Nockemann, P.; Pellens, M.; Binnemans, K. Influence of the Anion on the Electrical Conductivity and Glass Formation of 1-butyl-3-methylimidazolium Ionic Liquids. *J. Chem. Phys.* **2010**, *133*, 034503.
(52) Xu, W.; Wang, L. M.; Nieman, R. A.; Angell, C. A. Ionic Liquids of Chelated Orthoborates as Model Ionic Glassformers. *J. Phys. Chem. B* **2003**, *107*, 11749−11756.
(53) Angell, C. A. *Entropy Fragility Supercooling Liquids* **1997**, *102*, 171.
(54) Angell, C. A. Mobile Ions in Amourphous Solids. *Annu. Rev. Phys. Chem.* **1992**, *43*, 693−717.
(55) Böhmer, R.; Ngai, K. L.; Angell, C. A.; Plazek, D. J. Nonexponential Relaxations in Strong and Fragile Glass Formers. *J. Chem. Phys.* **1993**, *99*, 4201.
(56) Angell, C. A. Liquid Fragility and the Glass Transition in Water and Aqueous Solutions. *Chem. Rev.* **2002**, *102*, 2627−2650.
(57) Tokuda, H.; Tsuzuki, S.; Susan, M. A. B. H.; Hayamizu, K.; Watanabe, M. How Ionic are Room-Temperature Ionic Liquids? An Indicator of the Physicochemical Properties. *J. Phys. Chem. B* **2006**, *110*, 19593−19600.
(58) Sangoro, J. R.; Serghei, A.; Naumov, S.; Galvosas, P.; Kärger, J.; Wespe, C.; Bordusa, F.; Kremer, F. Charge Transport and Mass Transport in Iimidazolium-Based Ionic Liquids. *Phys. Rev. E* **2008**, *77*, 051202 1−4.
(59) Tokuda, H.; Hayamizu, K.; Ishii, K.; Susan, M. A. B. H.; Watanabe, M. Physicochemical Properties and Structures of Room Temperature Ionic Liquids. 2. Variation of Alkyl Chain Length in Imidazolium Cation. *J. Phys. Chem. B* **2005**, *109*, 6103−6110.
(60) Bigi, A.; Cojazzi, G.; Panzavolta, S.; Rubini, K.; Roveri, N. Mechanical and Thermal Properties of Gelatin Films at Different Degrees of Glutaraldehyde Crosslinking. *Biomaterials* **2001**, *22*, 763−768.
(61) Krause, C.; Sangoro, J. R.; Iacob, C.; Kremer, F. Charge Transport and Dipolar Relaxations in Imidazolium-Based Ionic Liquids. *J. Phys. Chem. B* **2010**, *114*, 382−386.
(62) Shoifet, E.; Huth, H.; Verevkin, S.; Schick, C. 7th International Discussion Meeting on Relaxations in Complex Systems, Barcelona, July 2013. In Influence of cation size on dynamic glass transition in room temperature ionic liquids (Oral communication IL-18).
(63) Vila, J.; Varela, L. M.; Cabeza, O. Cation and Anion Sizes Influence in the Temperature Dependence of the Electrical Conductivity in Nine Imidazolium Based Ionic Liquids. *Electrochim. Acta* **2007**, *52*, 7413−7417.
(64) Xu, W.; Cooper, E. I.; Angell, C. A. Ionic Liquids: Ion Mobilities, Glass Temperatures, and Fragilities. *J. Phys. Chem. B* **2003**, *107*, 6170−6178.
(65) Viciosa, M. T.; Diogo, H. P.; Moura Ramos, J. J. The Ionic Liquid BmimBr: a Dielectric and Tthermal Characterization. *RSC Adv.* **2013**, *3*, 5663−5672.
(66) Cerveny, S.; Schwartz, G. A.; Alegría, A.; Bergman, R.; Swenson, J. Water Dynamics in n-propylene Glycol Aqueous Solutions. *J. Chem. Phys.* **2006**, *124*, 194−501.
(67) McCrum, N. G.; Read, B. E.; Williams, G. *Anelastic and Dielectric Effects Polymeric Solids*; Dover Publications: Mineola, NY, 1967; pp 108−111
(68) Macedo, P. B.; Moynihan, C. T.; Bose, R. Role of Ionic Diffusion in Polarization in Vitreous Ionic Conductors. *Phys. Chem. Glasses* **1972**, *13*, 171−179.
(69) Wübbenhorst, M.; van Turnhout, J. Analysis of Complex Dielectric Spectra. I. One-Dimensional Derivative Techniques and Three-Dimensional Modelling. *J. Non-Cryst. Solids* **2002**, *305*, 40−49.
(70) Howell, F. S.; Moynihan, C. T.; Macedo, P. B. Electrical Relaxations in Mixtures of Lithium-Chloride and Glicerol. *Bull. Chem. Soc. Jpn.* **1984**, *57*, 652−661.
(71) Pathmanathan, K.; Johari, G. P. Dipolar and Conductivity Relaxations in LiCl−Propylene Glycol Systems. *J. Chem. Phys.* **1991**, *95*, 5990.
(72) Polizos, G.; Tuncer, E.; Tomer, V.; Sauers, I.; Randall, C. A.; Manias, E. Dielectric Spectroscopy of Polymer-Based Nanocomposite Dielectrics with Tailored Interfaces and Structured Spatial Distribution of Fillers. In *Nanoscale Spectroscopy with Applications*; Musa, S. M., , Ed.; CRC Press: Boca Raton, FL, 2013.
(73) Moynihan, C. T.; Macedo, P. B.; Montrose, C. J.; Gupta, P. K.; DeBolt, M. A.; Dill, J. F.; Dom, B. E.; Drake, P. W.; Eastea, A. J. .l; Elterman, P. B.; Moeller, R. P.; Sasabe, H.; Wilder, J. A. Structural Relaxation in Vitreous Materials. *Ann. N. Y. Acad. Sci.* **1976**, *279*, 15−35.
(74) Sjöström, J.; Mattsson, J.; Bergman, R.; Johansson, E.; Josefsson, K.; Swenson, J. Dielectric Secondary Relaxation of Water in Aqueous Binary Glass-Formers. *Phys. Chem. Chem. Phys.* **2010**, *12*, 10452−10456.
(75) Tyagi, M.; Murthy, S. S. N. Dynamics of Water in Supercooled Aqueous Solutions of Glucose and Poly(ethylene glycol)s as Studied by Dielectric Spectroscopy. *Carbohydr. Res.* **2006**, *341*, 650−62.
(76) Ngai, K. L.; Paluch, M. An Extended Coupling Model Description of the Evolution of Dynamics with Time in Supercooled Liquids. *J. Phys.: Condens. Matter* **2003**, *15*, S1107.
(77) Ngai, K. L.; Paluch, M. Classification of Secondary Relaxation in Glass-Formers Based on Dynamic Properties. *J. Chem. Phys.* **2004**, *120*, 857−873.
(78) Kohlrausch, R. Theorie des electrischen Ruckstandes in der Leidener Flasche. *Ann. Phys. (IV)* **1854**, *1*, 79−86.
(79) Kohlrausch, R. Nachtrag uber die elastische Nachwirkung beim Cocon und Glasfaden. *Ann. Phys. (III)* **1847**, *12*, 393−399.
(80) Williams, G.; Watts, D. C. Non-Symmetrical Dielectric Relaxation Behaviour Arising from a Simple Empirical Decay Function. *Trans. Faraday Soc.* **1970**, *66*, 80−85.

(81) Alegria, A.; Guerrica-Echevarria, L. E.; Goitiandia, I. T.; Colmenero, J. α-Relaxation in the Glass Transition Range of Amorphous Polymers. 1. Temperature Behavior across the Glass Transition. *J. Macromol.* **1995**, *28*, 1516−1527.
(82) Kudlik, A.; Tschirwitz, C.; Blochowicz, T.; Benkhof, S.; Rössler, E. Slow Secondary Relaxation in Simple Glass Formers. *J. Non-Cryst. Solids* **1998**, *235*−*237*, 406−411.
(83) Ngai, K.; Capaccioli, S. Relation Between the Activation Energy of the Johari-Goldstein β relaxation and T_g of glass formers. *Phys. Rev. E* **2004**, *69*, 031501 1−5.
(84) Rivera, A.; Rössler, E. Evidence of Secondary Relaxations in the Dielectric Spectra of Ionic Liquids. *Phys. Rev. B* **2006**, *73*, 1−4.